Real-time x-ray studies of gallium nitride nanodot formation by droplet heteroepitaxy

Yiyi Wang, Ahmet S. Özcan,[a] Christopher Sanborn, and Karl F. Ludwig[b]
Physics Department, Boston University, Boston, Massachusetts 02215, USA

Anirban Bhattacharyya, Ramya Chandrasekaran, and Theodore D. Moustakas
Department of Electrical and Computer Engineering, Boston University, Boston, Massachusetts 02215, USA

Lin Zhou and David J. Smith
Department of Physics, Arizona State University, Tempe, Arizona 85287, USA and School of Materials, Arizona State University, Tempe, Arizona 85287, USA

(Received 24 April 2007; accepted 10 August 2007; published online 11 October 2007)

Self-organized gallium nitride nanodots have been fabricated using droplet heteroepitaxy on *c*-plane sapphire by plasma-assisted molecular beam epitaxy at different substrate temperatures and Ga fluxes. Nanoscale Ga droplets were initially formed on the sapphire substrate at high temperatures by Ga deposition from an effusion cell in an ultrahigh vacuum growth chamber. Subsequently, the droplets were converted into GaN nanodots using a nitrogen plasma source. The process was monitored and controlled using real-time grazing-incidence small-angle x-ray scattering. The samples were examined postgrowth by *in situ* grazing incidence x-ray diffraction and reflection high-energy electron diffraction, which confirmed the epitaxial relationship between the GaN nanodots and the sapphire surface. X-ray diffraction indicated that the wurtzite phase was dominant at higher substrate temperature (710 °C), but a mixture of wurtzite and zinc blende phases was present at a substrate temperature of 620 °C. *Ex situ* atomic force microscopy and transmission electron microscopy analyses showed that the dot size distribution was bimodal. A thin GaN continuous layer of ~ three monolayers thick was observed by transmission electron microscopy on the sample grown at a substrate temperature of 620 °C, but no such layer was observed for the substrate temperature of 710 °C. This suggests that there is little mobility of Ga atoms in contact with the sapphire substrate at the lower temperature so that they cannot easily diffuse to nearby droplets and instead form a thin layer covering the surface. © *2007 American Institute of Physics*. [DOI: 10.1063/1.2786578]

I. INTRODUCTION

III-V nitride semiconductor quantum dots (QDs) have promising applications in optoelectronic and electronic devices,[1] such as quantum dot lasers,[2] quantum dot photodetectors,[3] and single electron transistors.[4] Manufacturing QDs over large areas can be challenging using conventional lithographic techniques, which involve sophisticated processing steps. Therefore, self-organized QD synthesis methods have attracted considerable attention for nanotechnology applications due to their simple and cost-effective processing.

In order to fabricate GaN QDs, most previous studies have utilized strain-driven three-dimensional (3D) growth methods, in which the dots were typically grown under compressive stress either in the Stranski-Krastanov (SK) growth mode or some variations.[5–7] These techniques require a large lattice mismatch between the growing layer and the substrate to achieve elastic relaxation. The widely used growth procedure employs the deposition of a strained two-dimensional wetting layer that undergoes elastic relaxation through the formation of QDs. As a result, GaN QDs are usually formed on thin GaN wetting layers. QD formation utilizing the SK growth mode has been demonstrated by molecular beam epitaxy (MBE) and metal-organic chemical vapor deposition (MOCVD). In addition, nitride QD formation has been reported on nearly lattice-matched substrates using antisurfactants such as Si.[8]

As an alternative approach to the SK-type QD formation method, some recent MOCVD and gas-phase MBE growth studies have adopted the droplet heteroepitaxy technique to fabricate GaN nanodots.[9,10] Droplet heteroepitaxy by MOCVD is based on forming Ga nanodroplets deposited by a vapor source and subsequent nitridation of the droplets at high temperatures using ammonia.

In this work, we have investigated droplet heteroepitaxy as a function of the substrate temperature and Ga flux. The method is based on forming self-organized Ga nanodroplets during Ga deposition from an effusion cell and subsequent conversion into GaN nanodots by nitridation using a plasma source. The growth process was monitored by real-time grazing incidence small-angle x-ray scattering (GISAXS) using intense x-rays from a synchrotron source. Postgrowth samples were analyzed by reflection high-energy electron

[a]Present address: IBM Microelectronics, East Fishkill, NY.
[b]Author to whom correspondence should be addressed. Electronic mail: ludwig@buphy.bu.edu

TABLE I. Table of growth conditions of samples A, B, C and D.

Sample	A	B	C	D
Substrate temperature (°C)	710	680	620	620
Ga cell temperature (°C)	1064	1064	1064	1005

diffraction (RHEED), grazing incidence x-ray diffraction (GID), atomic force microscopy (AFM), and transmission electron microscopy (TEM).

II. EXPERIMENTAL DETAILS

The growth experiments were performed in an ultrahigh vacuum (UHV) x-ray diffraction chamber with a base pressure of 10^{-9} Torr. A dual filament Applied Epi SUMO effusion cell was employed for Ga deposition and a UNI-Bulb rf plasma source from Applied Epi-Veeco, operated at 300 W, was used for nitridation. The nitrogen flow rate was 0.8 SCCM (SCCM denotes standard cubic centimeter at STP) and the chamber pressure was 1.0×10^{-5} Torr during nitridation. The exposures of the Ga beam and the nitrogen plasma were adjusted by remotely controlled shutters.

Results from four samples are described, which are labeled here as samples A, B, C, and D. The sapphire samples were small cuts from "epitaxial" quality commercial wafers with *c*-plane surface orientation. The samples were back-coated with a 0.5-μm thick Ti film for effective heating and optical monitoring of temperature. The sample temperature was monitored by a pyrometer and the heater was controlled by a thermocouple at the back of the sample holder. The four samples were processed in the Ga-rich condition and the growth conditions are listed in Table I. Samples A, B, and C were processed at a Ga cell temperature of 1064 °C and substrate temperatures of 710, 680, and 620 °C, respectively. In order to study the formation of GaN nanodots at a lower Ga cell temperature (lower flux), sample D was processed at a substrate tempereature of 620 °C in order to remain in the Ga droplet regime for a Ga effusion cell temperature of 1005 °C. Prior to Ga deposition, the substrates were degassed by annealing in UHV at 800 °C for at least 30 mins. The surface quality of each sample was assessed by RHEED before deposition; all RHEED patterns indicated a smooth unreconstructed surface.

The x-ray experiments were performed on beamline X21 at the National Synchrotron Light Source at Brookhaven National Laboratory. More details about this real-time surface x-ray characterization facility for dynamic processing are described elsewhere.[11] An incident photon energy of approximately 10.40 keV was used with a flux of 2.0×10^{12} photons per second using a nondispersive Si (111) double-crystal monochromator with a beam size of 0.5×0.5 mm^2 at a storage ring current of 300 mA.

The GISAXS geometry used in our experiments is shown in Fig. 1. The GISAXS technique[12] is sensitive to nanometer-size morphological changes on the surface, such as roughening and island formation. Since GISAXS is a non-invasive scattering technique, it is an ideal real-time tool to monitor liquid surfaces and droplets. Typically, GISAXS measurements can monitor lateral surface correlations with

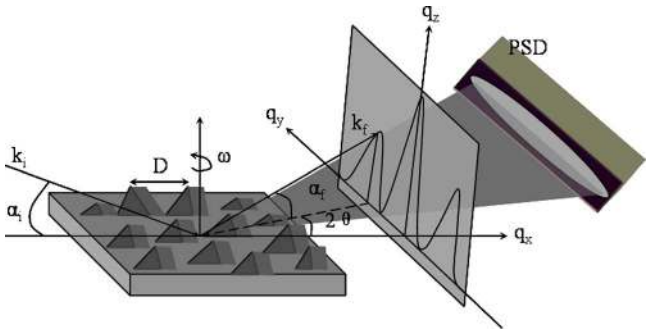

FIG. 1. Schematic of GISAXS geometry. Wavevectors $\mathbf{k}_i$ and $\mathbf{k}_f$ are the incident and scattered wave vectors, respectively. The linear position-sensitive detector is oriented parallel to the sample surface.

length scales between 1 and 250 nm. The scattering intensity was collected in real time by a one-dimensional (1D) position-sensitive detector (PSD) with 1 s time resolution in a vertical geometry. For the real-time GISAXS scans, the incidence angle was kept constant at 1°, while the exit angle was near the critical angle (0.2°) to the sample surface to enhance the surface sensitivity. The asymmetric scattering geometry was chosen to avoid going directly through the specular rod itself. Instead, the GISAXS passes through the tail of the specular rod and $q_{\|}$, the wavenumber transfer parallel to the surface, can be small (0.005 nm^{-1}), but never zero. We will refer to the GISAXS peak near $q_{\|}=0$ as the "near-specular" peak.

The x-ray geometry for GID measurements is shown in Fig. 2. Both the incidence angle α_i and exit angle α_f were kept constant at approximately 0.5° to enhance surface sensitivity. The in-plane GID scans were performed along the GaN $[l0\bar{l}0]$ direction, which includes the angular range of the sapphire $(11\bar{2}0)$ peak, GaN wurtzite $(10\bar{1}0)$ peak, and GaN zinc blende (111) peak.

In addition to x-rays, the surface was monitored by *in situ* RHEED analysis before and after the GaN nanodot formation. *Post mortem* AFM in the tapping mode was used to investigate the surface morphology. In addition, TEM studies were made in both plane-view and cross-section geometries with a JEM-4000EX high-resolution electron microscope (Cs=1.0 mm), equipped with a top-entry, double-tilt specimen holder. The samples were prepared for TEM observation by standard mechanical polishing and dimpling, followed by Ar ion milling.

III. RESULTS

A. Real-time GISAXS data

Real-time monitoring of the surface by x-ray scattering was crucial for controlling the process parameters, particu-

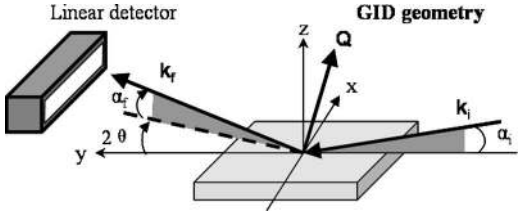

FIG. 2. Scattering geometry of GID. Q is the momentum transfer defined by α_i, α_f, and in-plane angle 2θ.

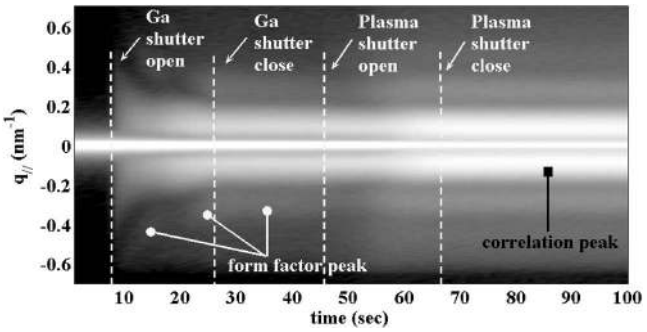

FIG. 3. Real-time GISAXS evolution of sample B during Ga deposition and subsequent plasma nitridation at 680 °C. The scan was taken at $q_z = 0.9$ nm^{-1}. Arrow with square head indicates intense peaks related to the lateral correlation length. Arrows with round heads indicate less intense peaks related to dot size.

larly the timing of the Ga deposition and the plasma nitridation of the Ga droplets. Figure 3 shows the GISAXS time evolution of sample B during Ga adsorption and subsequent nitridation at $q_z = 0.9$ nm^{-1} (momentum transfer normal to the sample surface). The x axis represents time, and the y axis represents the momentum transfer parallel to the sample surface $q_{\|}$. The sapphire substrate temperature was kept constant at 680 °C throughout the process. The Ga cell temperature was 1064 °C and the total exposure of Ga for acquiring the data shown in Fig. 3 was 20 s. Initially, the scattering profile shows only the intensity of the near-specular reflection (at $q_{\|} \approx 0$) from the sapphire substrate surface. After the Ga shutter is opened, two kinds of peaks appear symmetrically on each side of the central peak. The positions of the high intensity peaks (indicated by square-headed arrow at smaller $q_{\|}$ value), which we call the correlation peaks, are related to the distance between laterally correlated Ga droplets. The positions of the peaks indicated by round-headed arrows at larger $q_{\|}$ value with low intensity, which we call the form factor peaks, are related to the size of Ga droplets with high uniformity, i.e., they are the peaks associated with the internal structure and shape of the dots. During Ga deposition, both the droplet correlation and droplet form factor peaks grew and shifted towards a small $q_{\|}$ value. The behavior of the form factor peaks suggests an improvement of droplet uniformity and growth in droplet size; the behavior of the correlation peaks suggests an improvement of correlation in the lateral direction and an increase in the lateral correlation length which might be due to droplet coalescense.

These observations can be seen more clearly in Fig. 4(b), which shows snapshots of the GISAXS time evolution from Fig. 3. The x axis denotes the momentum transfer parallel to the sample surface $q_{\|}$. The y axis denotes the normalized x-ray scattering intensity. Arrows indicate the directions in which the peaks are evolving during growth. Figure 4(b) also indicates that both kinds of peaks continued to evolve with further coarsening after the Ga shutter was closed but at a

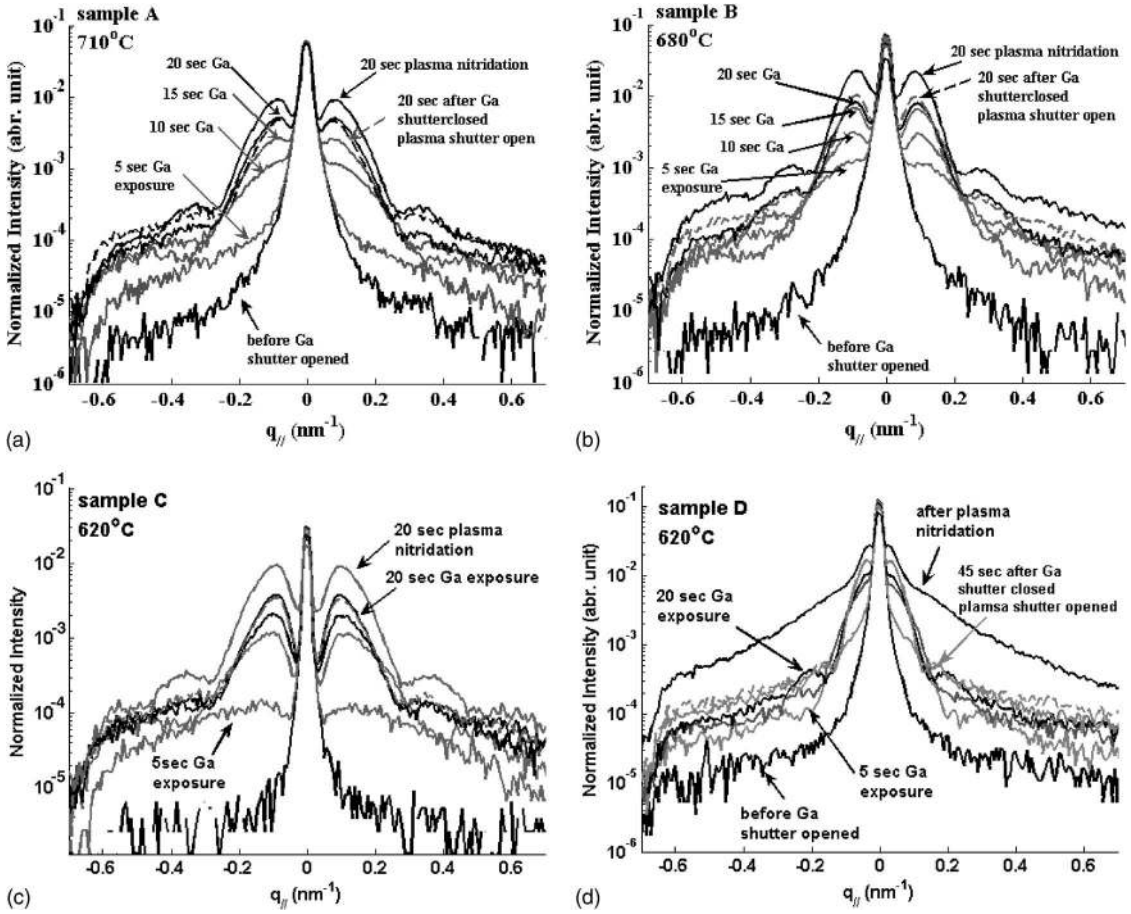

FIG. 4. Selected slices from real-time GISAXS evolution during Ga droplet formation and subsequent nitridation of (a) sample A at substrate temperature 710 °C and Ga cell temperature 1064 °C, (b) sample B at substrate temperature 680 °C and Ga cell temperature 1064 °C, (c) sample C at substrate temperature 620 °C and Ga cell temperature 1064 °C, and (d) sample D at substrate temperature 620 °C and Ga cell temperature 1005 °C.

TABLE II. GaN nanodot size information from GISAXS, AFM, and TEM analyses.

Sample	A	B	C	D
Substrate temperature (°C)	710	680	620	620
Ga cell temperature (°C)	1064	1064	1064	1005
Lateral correlation length of large dots from GISAXS large peaks (nm)	79	74	70	230
Dot diameter of large dots from GISAXS small peaks (nm)	31	37	29	
Large dot density from GISAXS (nm)	1.6×10^{10}	1.8×10^{10}	2.0×10^{10}	1.9×10^{9}
Large dot size from Fourier transform of GISAXS (nm)	30	35	28	30
Large dot density from AFM (nm)	1.4×10^{10}	2.6×10^{10}	3.4×10^{10}	3.5×10^{9}
Large dot size from AFM (nm)	41	47	42	
Large dot height from AFM (nm)	2.4	2.4	2.7	
Large dot size from TEM (nm)		30		
Large dot height from TEM (nm)		3–3.5		

much slower rate than during Ga deposition. As soon as the surface was exposed to the active species from the nitrogen plasma, both kinds of peaks were enhanced without further coarsening. After 20 s of plasma nitridation, the GISAXS pattern stopped evolving and remained unchanged. The final position of the droplet correlation peak suggests that the average interdot distance is $2\pi/q_{\parallel}\sim74$ nm. The dot density calculated from the interdot distance is $\sim1.8\times10^{10}/\mathrm{cm}^{-2}$. The relationship between the droplet form factor peak position and average droplet size will vary slightly depending upon the droplet size distirubution and droplet shapes. *Post facto* AFM and TEM studies discussed below show that the nitridated droplets are relatively flat. For simplicity, we therefore assume that the square of the droplet form factor is approximately that of a flat circular disk, i.e., the Airy function. In this case, the disk diameter is related to the position of the first maximum of the scattered intensity as $d\approx3.27\pi/q_{\max}$.[13] The final position of the droplet form factor peak suggests that the average dot diameter is ~37 nm.

Figures 4(a) and 4(c) show snapshots of the GISAXS time evolution during the formation of GaN nanodots for samples A and C, which were grown at different substrate temperatures. Figure 4(d) shows the GISAXS profile of sample D, which was grown at a lower Ga cell temperature and lower substrate temperature, to study the influence of Ga flux on the GaN nanodot formation. As seen in Figs. 4(a) and 4(c), the two kinds of peaks (correlation and form factor) evolved in similar ways as that of sample B during Ga deposition. The GISAXS evolution of sample A was slower than that of sample B during Ga exposure. This result indicates slow surface evolution at relatively high substrate temperature, which could be due to the higher evaporation rate (i.e., lower net absorption rate) of Ga at a higher substrate temperature. As shown in Fig. 4(d), both the droplet correlation and droplet form factor peaks for sample D evolved in a similar fashion as these of samples A, B, and C during Ga exposure but appeared at much smaller $q_{\parallel}$ values indicating a larger droplet size and larger interdot distance. As soon as the surface was exposed to the nitrogen plasma, the intensity of the diffuse scattering part increased rapidly and the form factor peaks smeared out, suggesting surface roughening.

Table II lists the GaN nanodot size, interdot distance, and dot density derived from the final GISAXS patterns of the four samples. For samples A, B, and C grown at the same Ga flux but different substrate temperature, sample A with the highest substrate temperature has the lowest dot density, while sample C with the lowest substrate temperature has the highest dot density. The final dot size of sample B (680 °C) is the largest among the three samples. Our interpretation is that the Ga evaporation rate from the surface is lower at lower substrate temperature and the droplets will tend to grow larger than at higher substrate temperature. However, the diffusion rate is also slow at low substrate temperatures, which leads to less droplet coalescence. Therefore, the dots at a substrate temperature of 680 °C (sample B) are larger than those grown at either 710 °C (sample A) or 620 °C (sample C).

In order to obtain more information about the droplet mean lateral size, an approach based on small-angle scattering theory[14,15] can be used. The analysis relies on obtaining the real-space correlation function of the electron density by taking the Fourier transform of the GISAXS profile. The details of this analysis can be found in Ref. 16. The Fourier transform of the measured GISAXS profile in $q_{\parallel}$ is shown in Fig. 5, this is a radial distribution function. The central peak close to $r=0$ corresponds to the mean electron density distribution of individual droplets. Twice the half width at half maximum (HWHM) of this peak gives an approximate value for the droplet size. The peak at the tail part of the curve corresponds to the average distance between the dots. Figure 5 shows that the average size and dot distance of the larger dots increase for all samples during Ga exposure and plasma nitridation. The final dot sizes, which agree well with the analysis of the meansured GISAXS profiles, are listed in Table II.

B. *In situ* GID data

Figure 6 shows the in-plane radial GID scan pattern from sample B after nitridation of the Ga droplets. The presence of the wurzite $(10\bar{1}0)$ peak indicates that nitridation of the Ga droplets has produced wurtzite GaN nanocrystalline

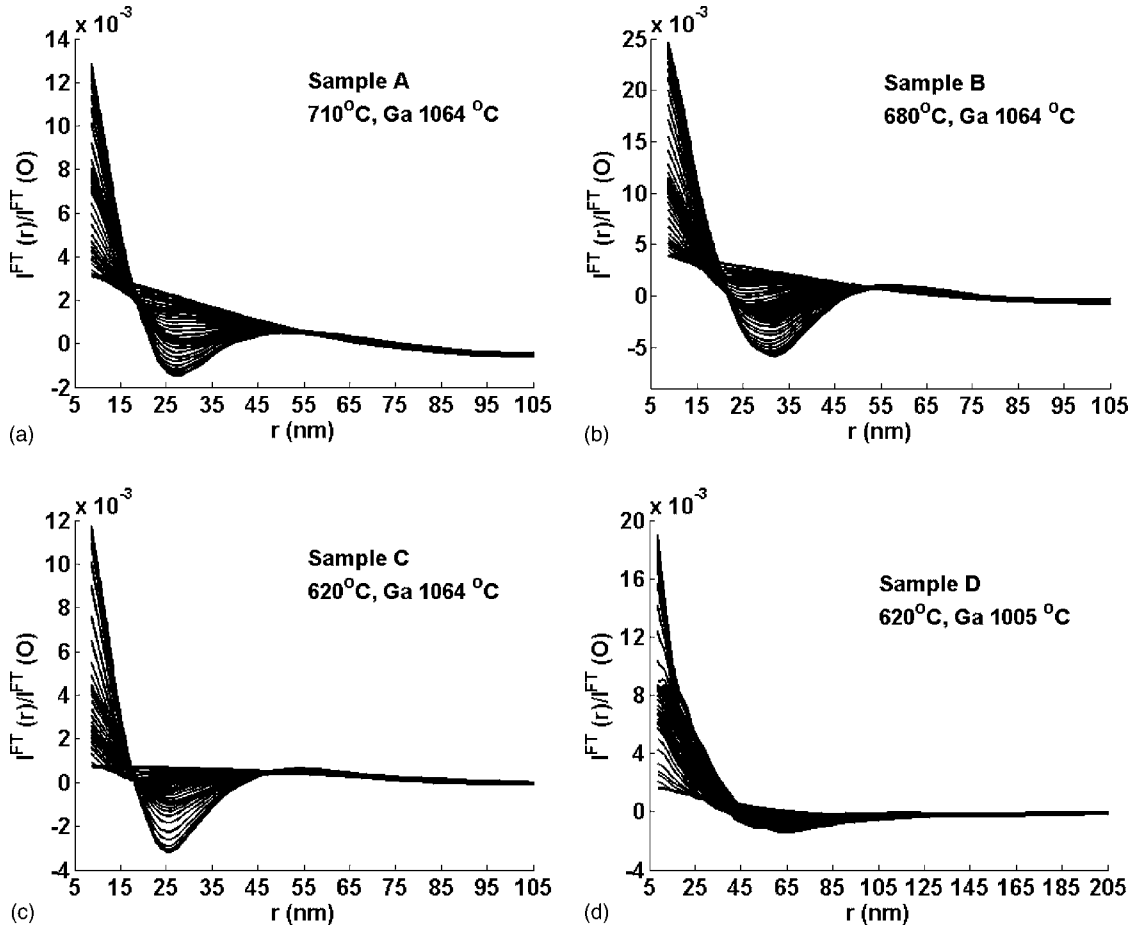

FIG. 5. Fourier transform of measured GISAXS each second during GaN nanodot formation, which gives approximately the real-space electron density correlation. The peak at larger r indicates the average spacing between droplets and the intensity decay at smaller r values corresponds to the electron density distribution of individual droplets.

nanodots which have a strong epitaxial relationship with the sapphire substrate. Further in-plane rocking-curve scans give a peak width of 1.5°, suggesting that the GaN nanodots are well oriented with respect to the substrate. The position of the observed GaN $(10\bar{1}0)$ peak is that expected for bulk GaN film, so that mismatch strain from the substrate is fully relaxed.

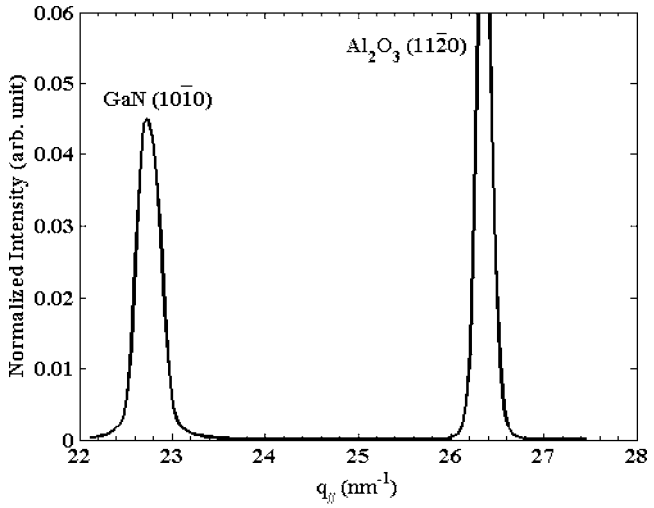

FIG. 6. In-plane grazing incidence x-ray diffraction (GID) of sample B along GaN $[10\bar{1}0]$ direction following GaN nanodot formation process.

The *in situ* x-ray GID patterns of samples A, B, C, and D are plotted together in log scale in Fig. 7. Similar to sample B, the GaN wurtzite peak positions are fully relaxed to the value of bulk GaN film for samples A, C, and D. However, the GID patterns of samples C and D show an additional GaN peak corresponding to the zinc blende phase of GaN, which probably grew because of the low substrate tempera-

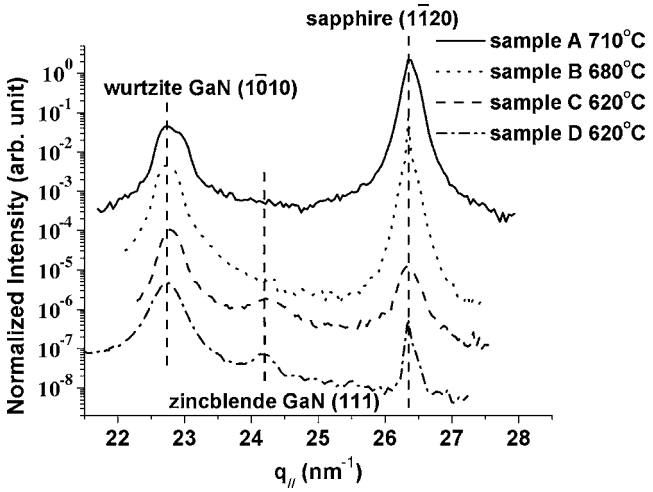

FIG. 7. In-plane grazing incidence x-ray diffraction (GID) of samples A, B, C, and D along the GaN $[10\bar{1}0]$ direction following the GaN nanodot formation process. Curves are rescaled for clarity.

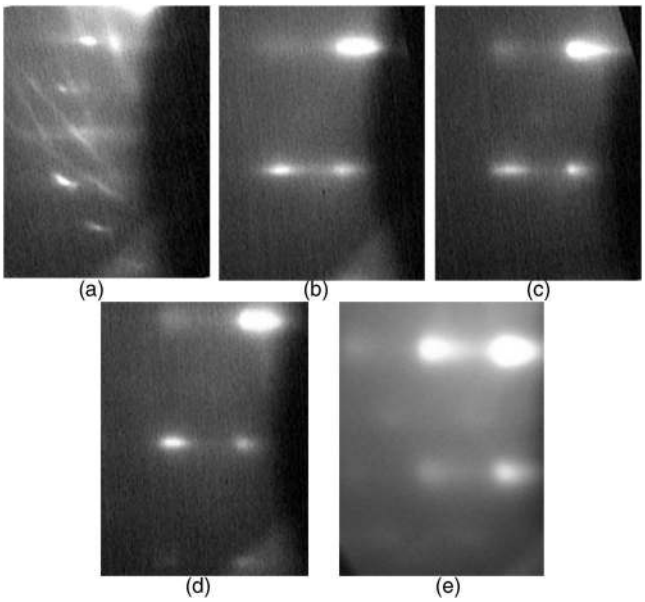

FIG. 8. RHEED patterns along the sapphire $\langle 11\bar{2}0\rangle$ azimuth: (a) before GaN nanodot formation showing smooth and unreconstructed sapphire surface, (b) sample A, (c) sample B, (d) sample C, and (e) sample D after GaN nanodot formation.

ture (620 °C). These results are discussed in the next section.

C. *In situ* RHEED data

Figure 8(a) shows the *in situ* RHEED pattern of sample A along the sapphire $\langle 11\bar{2}0\rangle$ azimuth after degassing and before the formation of GaN nanodots. The RHEED patterns of the other three samples before growth are all similar to the streaky pattern shown in Fig. 8(a), which indicate smooth and unreconstructed surfaces. After the formation of GaN nanodots, sapphire streaks disappear and new streaks form, which are the GaN $\{11\bar{2}0\}$ diffraction lines, as shown in Figs. 8(b)–8(e) for samples A, B, C, and D, respectively. This typical epitaxial alignment confirms that the GaN $[11\bar{2}0]$ direction is rotated by 30° with respect to the sapphire $[11\bar{2}0]$ direction.[17] The GaN RHEED streaks appear spotty which indicates a rough surface due to the presence of the nanodots. However, the RHEED diffraction pattern in Fig. 8(e) also clearly shows faint spots in between the spotty streaks, which suggests a rough surface with a mixure of wurtzite and zinc blende phases.

D. *Ex situ* AFM analysis

AFM analyses of all four samples are presented in the first column of Fig. 9 and second column for 0.5 and 3 μm lateral scan sizes, respectively. Figure 9(b1) for sample B (680 °C) clearly shows a bimodal distribution of GaN nanodot sizes with larger GaN dots on a background of smaller dots. The GaN nanodot sizes from AFM particle analysis of Fig. 9(b2) is shown in Fig. 9(b3), which gives the mean dot height of ~2.4 nm. The particle analysis also gives the average dot diameter of ~47.0 nm. These numbers are related to the large dots, which are visible in the AFM topographs. The small dots are probably too small and random to be analyzed statistically by the AFM software. This suggests that the GISAXS results are also likely to be dominated by scattering from the large dots. The large dot density of sample A counted from AFM image is approximately $2.6\times10^{10}/\mathrm{cm}^{-2}$, which is comparable to the GISAXS estimate $(1.8\times10^{10}/\mathrm{cm}^{-2})$.

The AFM analysis of sample A (710 °C) shows GaN nanodots directly on the sapphire substrate, visible in Figs. 9(a1) and 9(a2). The scratches that are commonly observed on sapphire substrates due to polishing can be observed in the background, which indicates the lack of a thick GaN layer. The AFM topograph of sample C 620 °C is similar to that of sample B (680 °C), but the small dots in the background are not as sharp as those of sample B, as shown in Fig. 9(c1). The results from the AFM histogram analysis of samples A and C are listed in Table II. Sample A has the lowest dot density $(1.4\times10^{10}/\mathrm{cm}^{-2})$, while sample C has the highest dot density $(3.4\times10^{10}/\mathrm{cm}^{-2})$ in agreement with the GISAXS data. Sample B has the largest dot size in diameter, while the dot heights are similar for the three samples.

The AFM topograph in Fig. 9(d) shows large GaN nanodots on a rough background of small GaN nanodots. The rough background might explain the high diffuse intensity in the GISAXS pattern. The dot density of the large dots from AFM analysis is $3.5\times10^{9}/\mathrm{cm}^{-2}$, which is the lowest among all four samples.

E. *Ex situ* TEM analysis

Plane-view and cross-section TEM analyses have been carried out to examine the structure of the GaN nanodots. The plane-view image of sample B in Fig. 10(a) shows a bimodal size distribution of GaN nanodots on the surface, which confirms the AFM results. Figure 10(b) shows the existence of both zinc blende and wurzite phase GaN nanodots. The coarse hexagonal arrays of fringes visible in Fig. 10(b) are Moiré fringes[18] caused by the overlap of GaN and sapphire lattice fringes. The average sizes of the large dots are approximately 30 nm in diameter. The high-resolution cross-sectional TEM image in Fig. 10(c) also shows the existence of both large and small GaN nanodots on the sapphire surface. Figures 10(d) and 10(e) show wurzite and zinc blende structures of GaN nanodots on sapphire with a height of approximately 3–3.5 nm. Both plane-view and cross-sectional TEM indicate that there is no GaN layer between the GaN nanodots and the sapphire substrate at this temperature (680 °C). Misfit dislocations were also observed at the GaN/sapphire interface, suggesting that the GaN nanodots were fully relaxed, which is consistent with the *in situ* GID results.

The TEM images of sample C in Fig. 11 show an obvious continuous GaN layer on the sapphire substrate, which is missing for sample B in Fig. 10. The continuous GaN layer is about three monolayers (MLs) thick in sample C. Figure 11(c) also indicates that the dot on the left-hand side grows along a direction other than the [0001] direction, as indicated by the arrow. The GaN nanodot on the right-hand side has a wurtzite structure with growth along the [0001] direction.

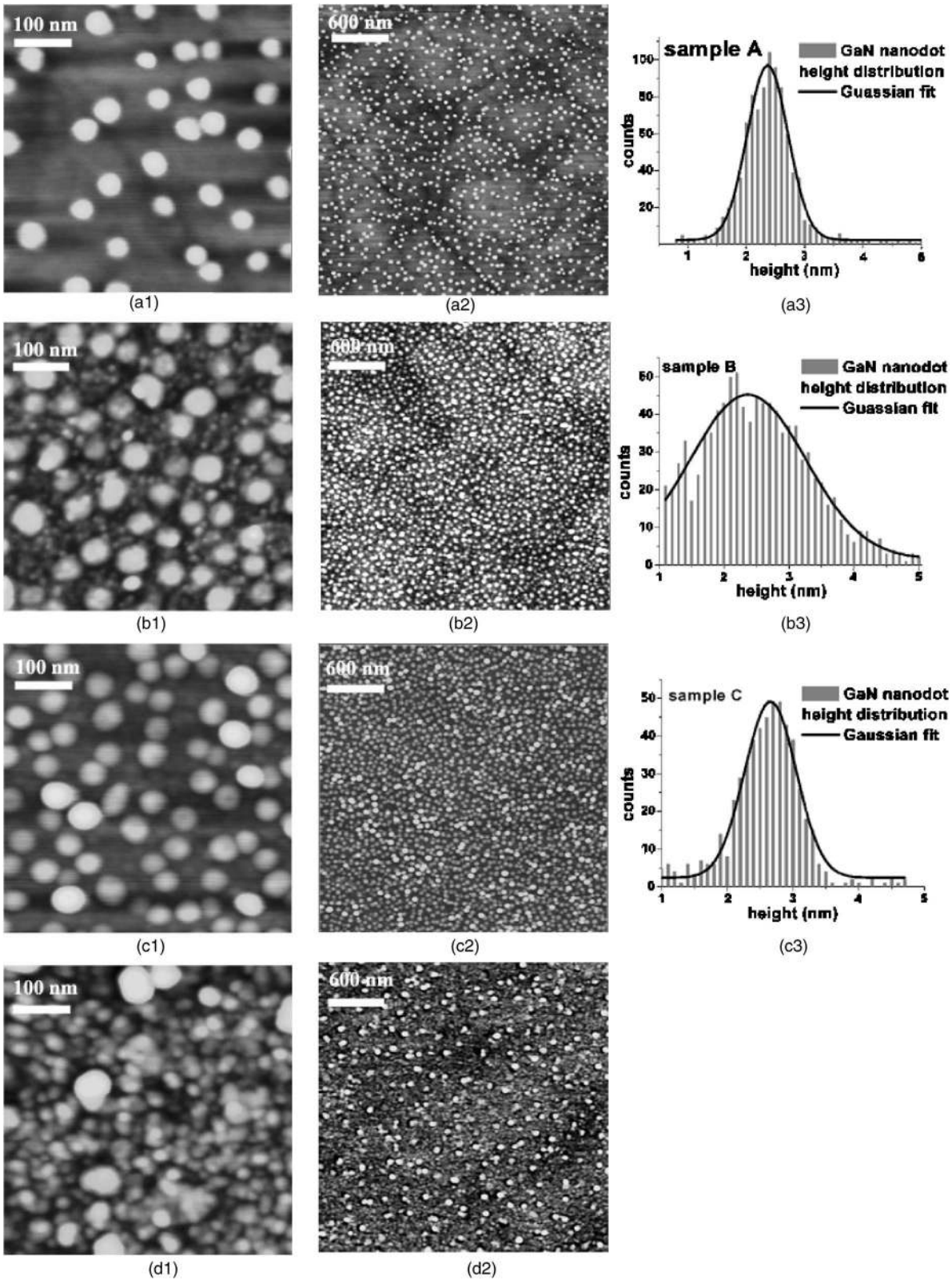

FIG. 9. The AFM analysis of sapphire samples with GaN nanodots: Column 1 shows 0.5×0.5 μm^2 size images; column 2 shows 3×3 μm^2 size images; column 3 shows histogram analyses from 3.0×3.0 μm^2 size AFM images; and y axis is the number of counts for the height of dot reflected on the x axis.

IV. DISCUSSION

A. Effect of substrate temperature and Ga flux on GaN nanodot formation

The large dot size and interdot distance depend on both the substrate temperature and the Ga cell temperature. The density of the nanodots can be controlled by varying either the substrate temperature or the Ga flux. In the Ga droplet regime, for the same Ga flux, the higher substrate temperature generates the lower density of nanodots, which we believe is due to the higher mobility at increased temperature.

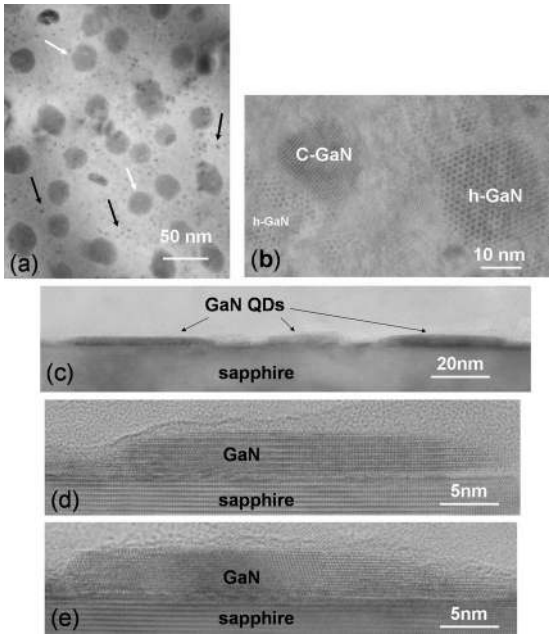

FIG. 10. [(a) and (b)] Plane-view TEM images of sample B taken on [0001] zone axis: (a) two sizes of GaN nanodots on sapphire surface, small dots indicated by black arrows and large dots indicated by white arrows, and (b) two kinds of dot crystallographic phases (hexagonal and cubic). [(c) and (d)] High-resolution cross-sectional TEM images taken on $[11\bar{2}0]$ zone axis: (c) coexistence of both large and small GaN nanodots; (d) and (e) show the wurzite and zinc blende structures of GaN nanodots with heights of approximately 3–3.5 nm.

At constant substrate temperature, the lower Ga flux generates a lower density of nanodots, which we believe is because of the smaller quantity of Ga available.

It is more difficult to control the dot size. Although the surface diffusion rate is high at high substrate temperature, the high Ga evaporation rate prevents the dot size from growing rapidly. At low substrate temperature, although droplets form rapidly, they cannot coalesce with nearby droplets and increase the average droplet volume easily. The GISAXS and AFM results show that the dot size of sample B, which was grown at an intermediate substrate temperature of 680 °C, is the largest among samples grown at constant Ga flux.

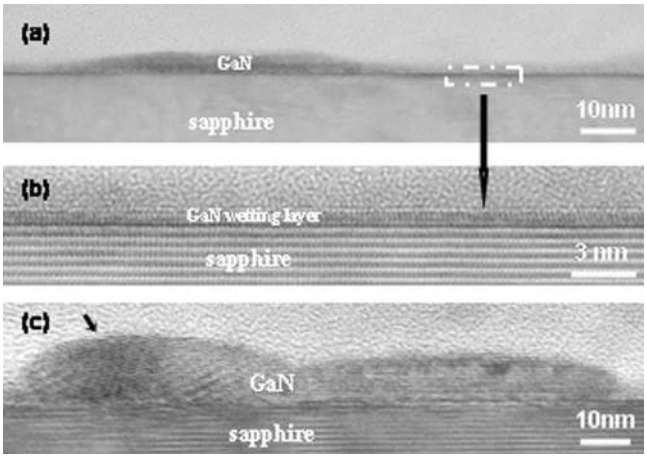

FIG. 11. High-resolution cross-sectional TEM images of sample C taken on $[11\bar{2}0]$ zone axis shows (a) GaN nanodot on sapphire substrate, (b) approximately 3 ML thick GaN wetting layer, and (c) different growth directions of GaN nanodot.

A continuous GaN layer approximately 3 ML thick is observed in sample C grown at low substrate temperature. Calculations of Ga adatoms on GaN have shown that a bilayer structure is particularly stable in that case.[19] We speculate that Ga in the layer forms sufficiently strong bonds that atoms are prevented from moving rapidly to the droplets at low temperatures. However, additional Ga adatoms on top of the continuous layer are still highly mobile even at the lowest temperature investigated and thus are able to move to the droplets.

It is well known that the III-V nitrides can exist in both the wurzite and zinc blende polymorphs.[17,20] We observed from x-ray GID scans, RHEED, and TEM that the wurzite GaN dots were dominant at high substrate temperature with a small distribution of cubic phase GaN dots, i.e., sample B. At low substrate temperature, the cubic phase GaN dots are more evident and there is a surface mixture of cubic and hexagonal phases in samples C and D. This is consistent with trends seen in the growth of GaN films.[20]

The epitaxial relationship of the GaN nanodots with the sapphire substrate suggests that the GaN crystallization starts at the droplet-sapphire interface. Therefore, the solidification of the Ga droplets by the nitrogen plasma may proceed in a manner similar to liquid-phase epitaxy, i.e., the reactive nitrogen species from the plasma source form a supersaturated solution in the Ga droplets and subsequently the droplets begin to crystallize at the substrate interface.[21,9] In cases where crystallization occurs first by direct reaction at the periphary of the droplets, a crater morphology is instead expected.[22]

Both the solubility and diffusivity of active nitrogen from the plasma source increase with temperature. At high substrate temperature, the Ga droplets can be rapidly converted into GaN nanodots by the nitrogen plasma. However, at slightly lower substrate temperature, the nitridation process starts before the nitrogen can reach the Ga-sapphire interface, which results in nonepitaxial orientations of the GaN, as indicated by the black arrow in Fig. 11(c).

B. Comparison with existing simulation and theory of droplet formation

Theoretical models of droplet formation on surfaces incorporate nucleation, coalesence, and ripening processes.[23–25] The droplets may nucleate heterogeneously at specific sites such as impurities on the surface or surface imperfections or they may nucleate homogeneously. Simulations of homogeneous droplet nucleation with growth and coalescence have shown the coexistence of monodispersed large droplets with polydispersed small droplets that form due to continuous nucleation.[25] However, simultaneous heteregenous nucleation results only in a monodispersed distribution of droplets. According to our AFM and TEM results, there is a bimodal distribution of droplet sizes for the four samples. The scattering peaks from the GISAXS data suggest that the larger size nanodots are highly uniform and

laterally correlated. These observations are qualitatively consistent with the simulation results for homogeneous nucleation, growth, and coalescence.

V. CONCLUSIONS

In conclusion, we have demonstrated that droplet heteroepitaxy by plasma-assisted MBE is a viable method for growing GaN nanodots on sapphire. Self-organized nanosize Ga droplets were formed on the sapphire surface at high temperatures by depositing Ga from an effusion cell. Comparing to previous theory/simulation models, our real-time results are consistent with the homogeneous nucleation, growth, and coalescence of droplets, in which a monodispersed distribution of droplet size emerges on a background of smaller polydisersed droplets. The Ga nanodroplets were converted into GaN nanodots by nitridation using a plasma source. The size and the density of the dots could be controlled by the Ga flux and the substrate temperature.

ACKNOWLEDGMENTS

We thank P. Siddons and R. France for their help with the experiments. This work was partially supported by DOE DE-FG02-03ER46037 and NSF DMR-0507351. The real-time x-ray system for surface processes was made possible by NSF DMR-0114154 and NSF DMR-0116567. The electron microscopy was supported by ONR Grant No. N-00014-04-1-0020. We acknowledge the use of facilities in the John M. Cowley Center for high resolution electron microscopy at Arizona State Univesity. "Data for this study were measured at beamline X21 of the National Synchrotron Light Source (NSLS). Financial support comes principally from the Offices of Biological and Environmental Research and of Basic Energy Sciences of the U.S. Department of Energy."

[1] C. Adelmann, J. Simon, G. Feuillet, N. T. Pelekanos, B. Daudin, and G. Fishman, Appl. Phys. Lett. **76**, 1570 (2000).
[2] W. W. Chow and H. C. Schneider, Appl. Phys. Lett. **81**, 2566 (2002).
[3] L. W. Ji, Y. K. Su, S. J. Chang, S. H. Liu, C. K. Wang, S. T. Tsai, T. H. Fang, L. W. Wu, and Q. K. Xue, Solid-State Electron. **47**, 1753 (2003).
[4] K. Kawasaki, D. Yamazaki, A. Kinoshita, H. Hirayama, K. Tsutsui, and Y. Aoyagi, Appl. Phys. Lett. **79**, 2243 (2001).
[5] B. Daudin *et al.*, Jpn. J. Appl. Phys., Part 1 **40**, 1892 (2001).
[6] B. Daudin *et al.*, Phys. Status Solidi A **176**, 621 (1999).
[7] N. Gogneau, D. Jalabert, E. Monroy, T. Shibata, M. Tanaka, and B. Daudin, J. Appl. Phys. **94**, 2254 (2003).
[8] S. Tanaka, M. Takeuchi, and Y. Aoyagi, Jpn. J. Appl. Phys., Part 2 **39**, L831 (2000).
[9] M. Gherasimova, G. Cui, S. R. Jeon, Z. Ren, D. Martos, J. Han, Y. He, and A. V. Nurmikko, Appl. Phys. Lett. **85**, 2346 (2004).
[10] C. W. Hu, A. Bell, F. A. Ponce, D. J. Smith, and I. S. T. Tsong, Appl. Phys. Lett. **81**, 3236 (2002).
[11] A. S. Özcan, Y. Wang, G. Ozaydin, H. Zhou, L. Zhou, R. Headrick, and K. F. Ludwig (unpublished).
[12] G. Renaud, R. Lazzari, C. Revenant, A. Barbier, M. Noblet, O. Ulrich, F. Leroy, J. Jupille, Y. Borensztein, C. R. Henry, J. P. Deville, F. Scheurer, J. Mane-Mane, and O. Fruchart, Science **300**, 1416 (2003).
[13] M. Born and E. Wolf, *Principles of Optics* (Cambridge University Press, Cambridge, 1980).
[14] A. Guinier, *X-Ray Diffraction: In Crystals, Imperfect Crystals and Amorphous Bodies* (Dover, Mineola, NY, 1994).
[15] B. E. Warren, *X-Ray Diffraction* (Dover, Mineola, NY, 1990).
[16] J. Stangl, V. Holy, P. Mikulik, G. Bauer, I. Kegel, T. H. Metzger, O. G. Schmidt, C. Lange, and K. Eberl, Appl. Phys. Lett. **74**, 3785 (1999).
[17] T. Lei, K. F. Ludwig, Jr., and T. Moustakas, J. Appl. Phys. **74**, 4430 (1993).
[18] D. B. Williams and C. B. Carter, *Transmission Electron Microscopy: A Textbook for Materials Science* (Plenum, New York, 1996).
[19] J. E. Northrup, J. Neugebauer, R. M. Feenstra, and A. R. Smith, Phys. Rev. B **61**, 9932 (2000).
[20] L. T. Romano, B. S. Krusor, R. Singh, and T. D. Moustakas, J. Electron. Mater. **26** (1997).
[21] T. D. Moustakas, J. P. Dismukes, S. E. Mohney, D. N. Buckley, S. J. Pearton, C. R. Abernathy, and W. D. Brown, *III-V Nitride Materials and Processes* (The Electrochemical Society, Pennington, NJ, 1998).
[22] T. Mano, K. Watanabe, S. Tsukamoto, H. Fujioka, M. Oshima, and N. Koguchi, J. Cryst. Growth **209**, 504 (2000).
[23] J. A. Blackman and S. Brochard, Phys. Rev. Lett. **84**, 4409 (2000).
[24] S. Ulrich, S. Stoll, and E. Pefferkorn, Langmuir **20**, 1763 (2004).
[25] F. Family and P. Meakin, Phys. Rev. A **40**, 3836 (1989).